

---

# NEST: Nested Event Stream Transformer for Sequences of Multisets

---

Minghui Sun\*<sup>1</sup> Haoyu Gong\*<sup>2</sup> Xingyu You<sup>1</sup>

Jillian Hurst<sup>3</sup> Benjamin Goldstein<sup>1</sup> Matthew Engelhard<sup>1</sup>

<sup>1</sup>Department of Biostatistics & Bioinformatics, Duke University

<sup>2</sup>Department of Biomedical Engineering, Duke University

<sup>3</sup>Department of Pediatrics, Duke University

{minghui.sun, m.engelhard}@duke.edu

## Abstract

Event stream data often exhibit hierarchical structure in which multiple events co-occur, resulting in a sequence of multisets (i.e., bags of events). In electronic health records (EHRs), for example, medical events are grouped into a sequence of clinical encounters with well-defined temporal structure, but the order and timing of events within each encounter may be unknown or unreliable. Most existing foundation models (FMs) for event stream data flatten this hierarchy into a one-dimensional sequence, leading to (i) computational inefficiency associated with dense attention and learning spurious within-set relationships, and (ii) lower-quality set-level representations from heuristic post-training pooling for downstream tasks. Here, we show that preserving the original hierarchy in the FM architecture provides a useful inductive bias that improves both computational efficiency and representation quality. We then introduce Nested Event Stream Transformer (NEST), a FM for event streams comprised of sequences of multisets. Building on this architecture, we formulate Masked Set Modeling (MSM), an efficient paradigm that promotes improved set-level representation learning. Experiments on real-world multiset sequence data show that NEST captures real-world dynamics while improving both pretraining efficiency and downstream performance.

## 1 Introduction

While originally designed for natural language sequence data [35, 27, 5], the Transformer’s ability to model complex categorical data dependencies and dynamics has inspired its widespread application to general event stream data, which are continuous-time sequences of complex, multi-modal events [22]. Transformer-based foundation models (FMs) have emerged as a transformative paradigm across diverse domains, enabling rapid adaptation to specialized downstream tasks through pretraining on large-scale data. In healthcare, electronic health records (EHR) data are represented as sequences of clinical events, from which FMs extract deep representations for clinical decision support [20, 38]. The same framework extends to commercial applications, where user purchase histories are encoded for next-item and next-basket recommendation [14, 34], and to financial domains, where real-time transaction streams are converted to deep features for fraud prevention [10].

We first define the term *multiset*, which is a *set with multiplicity*: an unordered collection that, unlike a standard set, permits duplicate elements. Event stream data frequently possesses a hierarchical

---

\* equally contributed

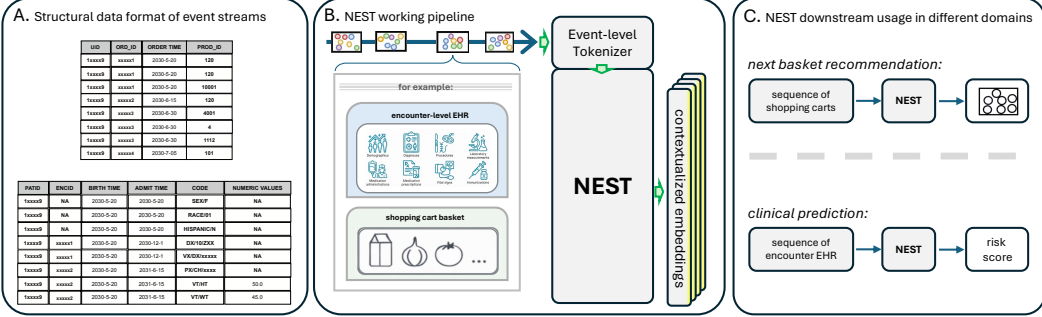


Figure 1: NEST models event stream data as sequences of multisets, where temporal order is preserved across sets and intra-set tokens are unordered. It is a domain-agnostic FM architecture that explicitly models set-level representations.

structure in which multiple events co-occur, forming a sequence of multisets. In the EHR domain, for example, medical events are grouped into encounters with clear temporal ordering, but the order of events *within* each encounter can be unknown, unreliable, or otherwise unimportant when modeling extended patient timelines. In this paper, we focus on modeling this data structure, which we term a **sequence of event multisets** (SeqSet): formally,  $\mathcal{H}_m = \{(\mathcal{X}_i, t_i)\}_{i=1}^m$ , where  $\mathcal{X}_i$  is a multiset of events occurring at time  $t_i$ .

Most FMs for event-stream data adopt the standard Transformer architecture due to its strong scalability and parallelization properties [20, 28, 18, 38, 23, 30]. However, this architecture does not naturally align with the structural characteristics of event streams that have hierarchical structure, as it does not explicitly or efficiently model their hierarchical ordering: multisets are temporally ordered at the sequence level, while tokens within each multiset are permutation-invariant.

First, GPT-style causal modeling [27] has achieved strong results in event-stream data modeling [22, 38, 30]. However, the autoregressive formulation forces the model to learn a specific token order, despite certain token groups being locally permutation-invariant. Secondly, BERT-style full self-attention [5] can preserve the temporal hierarchy, combining local permutation invariance within multisets with global sequential ordering across sets when time and set-level ordering are properly encoded, but it does so at substantial computational cost. This inefficiency severely constrains the effective context length, limiting the practical applicability to long event streams. Crucially, in these approaches representation learning is mainly driven by token-level optimization objectives such as masked language modeling (MLM) and next token prediction (NTP), and set-level representations are only inferred through pooling after the pretraining process. Prior work in textual domains has shown that heuristic post-training pooling of Transformer contextualized embeddings leads to inferior downstream performance [29, 6].

Therefore, we postulate that aligning the FM architecture and pretraining paradigm with the intrinsic inductive biases of the SeqSet data structure enhances both computational efficiency and representation learning.

Inspired by previous efforts in building hierarchical models for text data [40, 3] and event stream data [8, 21], we develop Nested Event Stream Transformer (NEST) as a foundation model suitable for event stream data. NEST adopts a simple and modular architecture built upon a stack of hierarchical Transformer layers. Each layer consists of a set-wise encoder (SWE) that models token-level interactions within sets, and a cross-set encoder (CSE) that captures dynamics across multisets at the whole sequence level, together enabling *dual-level contextualization*. By embedding the inductive bias of the hierarchical ordering in event streams into its architecture, this design offers two principal benefits: (i) enhanced computational efficiency via structurally induced sparse attention, and (ii) direct learning of set-level representations rather than relying on post hoc pooling.

Apart from the architectural modification, we also propose a separate pretraining objective, Masked Set Modeling (MSM), that is tailored for sequences of multisets and complements the standard MLM objective during NEST training. The MSM task enables NEST to produce ready-to-use set-level representations while retaining fine-grained token-level information, eliminating the need for heuristic post-training pooling.

We conduct extensive experiments across diverse event stream datasets from multiple real-world domains to evaluate NEST’s effectiveness. NEST achieves higher performance and improved computational efficiency compared to Transformer models trained on flattened event streams across multiple downstream tasks, including next basket recommendation and several clinically important prediction tasks. In addition, ablation studies demonstrate that the proposed MSM objective enhances set-level representation learning. To summarize, our contributions are as follows:

- We introduce **NEST**, a hierarchical Transformer foundation model for event-stream data that is computationally efficient and produces directly usable set-level representations without post-hoc aggregation.
- We formulate an **MSM** pretraining objective that complements the standard MLM to further refine set-level learning for improved downstream performance.
- To our knowledge, we are the first to propose a set-based FM approach for EHRs, which (i) explicitly preserves multiset boundaries in its architecture, and (ii) learns set-level representations through a pretraining procedure optimized for high computing efficiency.

## 2 Related Works

### 2.1 Hierarchical Transformer and Sparse Attention

Prior work in natural language processing has shown that hierarchical architectures are effective for modeling the inherent hierarchy of text data [2, 3, 7]. By leveraging this inductive bias, hierarchical models can achieve substantial efficiency gains over flat baselines, even when the latter are augmented with heuristic-based sparse-attention mechanisms [1, 41]. These gains largely stem from the structurally induced sparsity pattern in the attention mechanism.

In contrast, sparse attention has been less explored in event-stream foundation models, though several efforts have investigated hierarchical Transformers for event-stream data [21, 11]. These approaches also instantiate structurally induced sparse attention, though in different forms. However, the sliding-window attention mechanisms introduced in Longformer [1] and BigBird [41] do not align with the SeqSet event-stream structure, as window boundaries can split multisets (e.g., clinical encounters), breaking permutation invariance and fragmenting semantically coherent groups of events.

### 2.2 EHR Foundation Models

EHR foundation models are self-supervised models pretrained on EHR data for downstream clinical tasks. Early approaches such as BEHRT [20] and Med-BERT [28] adapted BERT-style MLM to structured EHR data, establishing strong baselines and proof of concept. Subsequent work has explored diverse pretraining objectives: CLMBR-T [38] and ETHOS [30] adopt autoregressive next token prediction; MOTOR [32] introduces time-to-event modeling for survival analysis; and EBCL [12] leverages event-based contrastive learning. Below we examine approaches most relevant to modeling long, structured medical sequences.

**Optimized Flat Transformers.** CORE BEHRT [23] systematically optimizes the flat BEHRT architecture through modern components such as Time2Vec [15], RoPE [33], and SwiGLU activations [31], establishing a strong baseline. Despite these optimizations, the flat architecture collapses all multisets into a single sequence, discarding the explicit hierarchy.

**Sliding-Window Hierarchical Architecture.** Hi-BEHRT addresses sequence length limitations through a two-stage architecture: a local encoder processes fixed-size sliding windows, and a global aggregator combines segment representations via BYOL-based contrastive pretraining [21]. However, window boundaries can split multisets, fragmenting semantically coherent event groups.

**Graph-Sequence Hybrid Architecture.** GT-BEHRT combines GNN-learned concept embeddings from a medical knowledge graph with a sequence Transformer for temporal modeling [24]. The GNN captures ontological relationships that are difficult to learn from co-occurrence alone, but this design requires an external knowledge graph, limiting generalizability.

**Hierarchical Transformer with Relational Embeddings.** HEART [11] introduces heterogeneous relation embeddings to capture type-specific pairwise correlations between clinical entities. While

expressive, the construction of pairwise embeddings incurs  $O(N^2)$  memory complexity, limiting scalability to long sequences, where  $N$  is the number tokens in the sequence.

**NEST’s Distinctions.** NEST directly models the nested SeqSet structure: SWE processes concurrent events as unordered multisets (without intra-set position embeddings), while CSE captures temporal dynamics across sets via RoPE. While individually standard Transformer layers, their interleaved composition yields structured sparse attention tailored to SeqSet data. Unlike Hi-BEHT, NEST respects multiset boundaries rather than imposing fixed-size windows. Unlike HEART, NEST achieves efficiency through architectural sparsity rather than explicit pairwise modeling. And unlike all prior approaches, NEST introduces MSM for explicit set-level representation learning.

### 2.3 Set-level Representation

Learning effective set-level representations is a key challenge for modeling event stream data. Naive strategies, such as mean-pooling or using standard [CLS] embeddings, typically struggle in downstream applications [29]. Self-supervised contrastive learning approaches have successfully enhanced BERT’s capability to learn sentence-level representations, which refine [CLS] embeddings, significantly improving outcomes in downstream tasks [29, 6, 4]. Notably, the contrastive loss does not explicitly relate the [CLS] token to other tokens; the connection arises only implicitly through self-attention.

However, these methods treat sentences as isolated instances. By contrast, in modeling event stream data, our goal is to enhance representation learning at the multiset level while capturing temporal dynamics across multisets within a sequence. SoftCLT [17], a plug-and-play method for time series contrastive learning, can be adapted to longitudinal multiset representations by treating [CLS] token embeddings as multivariate time series. However, contrastive objectives still provide only implicit pressure for [CLS] to summarize set contents.

Alternatively, the [CLS] representation can be explicitly tied to the corresponding multiset tokens through a set prediction task [37, 42], providing direct supervision for set-level summarization. NEST adopts this explicit approach via MSM (Section 3.4); we also evaluate contrastive alternatives in Section 4.3.

## 3 Method

### 3.1 Event Stream as a Sequence of Sets

We model an event stream as a **time-ordered sequence of unordered multisets**, where each multiset contains events, possibly with multiplicity, occurring at the same time. We pad and truncate the multisets and the overall sequence to fixed sizes: multiset size  $n$  and number of multisets  $m$ . Each event is a token. We denote the event stream for an arbitrary subject as  $\mathcal{H}_m = \{(\mathcal{X}_i, t_i)\}_{i=1}^m$ , where  $\mathcal{X}_i$  is a multiset of events at time  $t_i$  and  $m$  is number of multisets in the event stream. Each multiset includes a [CLS] token  $\mathbf{x}_{i,0}$ ; its embedding  $\mathbf{x}_{i,0}$  serves as the multiset representation.

In the following derivation,  $[\cdot]$  denotes column-wise stacking of a set of embedding vectors into a matrix. We use  $X_i^{(l)} = [\{\mathbf{x}_{i,j}^{(l)}\}_{j=1}^n] \in \mathbb{R}^{d_{\text{model}} \times n}$  to represent the (contextualized) embeddings of tokens in  $\mathcal{X}_i$ , where  $\mathbf{x}_{i,j}^{(h)}$  is the embedding or hidden states of token  $\mathbf{x}_{i,j}$ . The sequence  $\{X_i^{(h)}\}_{i=1}^m$  serves as the input to each Transformer layer.

### 3.2 Components of NEST

Transformer layers are the core building blocks of foundation models, directly shaping both computational efficiency and representation quality. NEST adapts the interleaved variant of Hierarchical Attention Transformer (HAT) [3], originally developed for long-document NLP, for event-stream modeling.

Each NEST layer consists of a Set-Wise Encoder (SWE) followed by a Cross-Set Encoder (CSE). Within a single layer, direct attention between tokens from different multisets is disallowed; instead, information exchange occurs either within each set through the SWE, or via the [CLS] tokens

through the CSE. However, global cross-set interactions emerge indirectly across the network as the information propagates through the [CLS]-mediated bridges.

Although both SWEs and CSEs employ dense attention, their composition effectively yields a sparse attention pattern at the layer level. This hierarchical design (i) induces sparse token-level interactions, and (ii) facilitates to learn set-level representations through dual-level contextualization across the series of SWE-CSE blocks. Figure 2 illustrates the resulting attention pattern within a NEST layer. Numerous refinements have been proposed since the earliest generation of Transformers [35, 5]. We

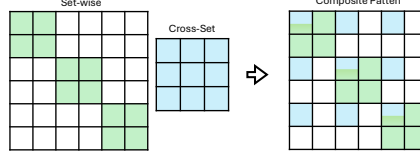


Figure 2: Dense attention is applied both within and across sets, yet their composition yields a sparse pattern in each NEST layer. The theoretical complexity of the composite pattern is  $O(nN + m^2) = O(nN)$ , where  $N = mn$  is the context window size.

adopt a modern Transformer design in NEST, incorporating bias-free linear projections (i.e.,  $Q$ ,  $K$ , and  $V$ ) and normalization layers [36], Pre-LayerNorm [39], SwiGLU activations [31], and Rotary Position Embeddings (RoPE) [33].

Following the established approaches to temporal modeling in EHR foundation models [20, 28, 23], we combine Time2Vec (T2V) [15] with RoPE to encode both the absolute time of tokens (e.g., age) and their positions within the event stream. Specifically, T2V provides absolute time embeddings that are added to the input embeddings before being passed into the Transformer. To preserve within-set ordering invariance, RoPE is applied only for multiset position encoding via the CSE in each NEST layer. Figure 3 provides a schematic overview of the model architecture.

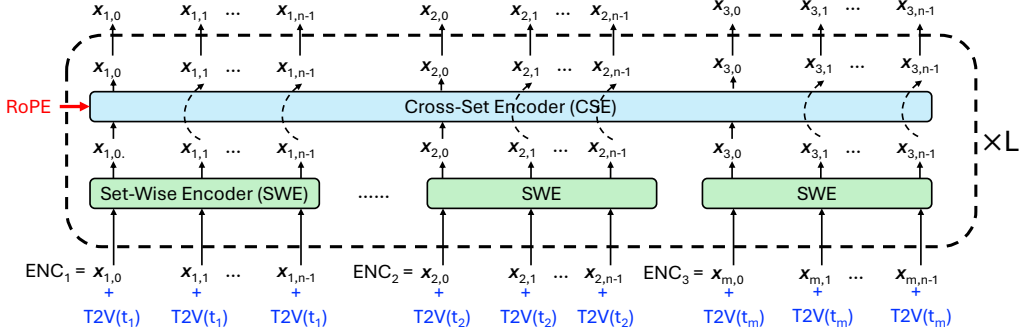


Figure 3: NEST is a simple stack of hierarchical Transformer layers. Each layer is a composite Transformer block that integrates a Set-Wise Encoder (SWE) with a Cross-Set Encoder (CSE). T2V is used for absolute time encoding, and RoPE is used in each CSE for position encoding at the multiset-level.

### 3.3 Dual-level Contextualization

Within each multiset, token interactions are confined to the set, so the [CLS] token carries set information via **set-wise** contextualization. Across the sequence, [CLS] tokens exchange information through **cross-set** contextualization.

The **set-wise** contextualization happens within each set independently. Given the multiset  $\mathcal{X}_i$ ,

$$\begin{aligned} \mathbf{x}_{i,j}^{(l+1)} &\leftarrow \mathbf{x}_{i,j}^{(l)} + \\ &\sum_h \mathbf{W}_O^{(l,h)} \mathbf{V}_i^{(l,h)} \text{Softmax} \left( \frac{1}{\sqrt{d_k}} \mathbf{K}_i^{(l,h)\top} \mathbf{q}_{i,j}^{(l,h)} \right) \\ \mathbf{V}_i^{(l,h)} &= \mathbf{W}_V^{(l,h)} \mathbf{X}_i^{(l)} = [\{\mathbf{v}_{i,j}^{(l,h)}\}_{j=1}^n] \\ \mathbf{K}_i^{(l,h)} &= \mathbf{W}_K^{(l,h)} \mathbf{X}_i^{(l)} = [\{\mathbf{k}_{i,j}^{(l,h)}\}_{j=1}^n] \end{aligned} \quad (1)$$

$\mathbf{V}_i^{(l,h)}$  and  $\mathbf{K}_i^{(l,h)}$  are the layer- and head-specific value and key matrices for the tokens in  $\mathcal{X}_i$ , respectively, and  $\mathbf{q}_{i,j}^{(l,h)} = \mathbf{W}_Q^{(l,h)} \mathbf{x}_{i,j}^{(l)}$  is the layer- and head-specific query vector of token  $j$ .  $\mathbf{W}_O^{(l,h)}, \mathbf{W}_Q^{(l,h)}, \mathbf{W}_K^{(l,h)}, \mathbf{W}_V^{(l,h)} \in \mathbb{R}^{d_{\text{model}} \times d_k}$  are the head-specific projection matrices in multi-head attention of **SWE**. Notably, inside each hierarchical Transformer layer, **SWE** is shared across all multisets in the sequence.

On the other hand, the **cross-set** contextualization operates solely on  $\{\mathbf{x}_{i,0}\}_{i=1}^m$ , which is the collection of all **[CLS]** tokens in the event stream  $\mathcal{H}_m$ . The hidden states of the other tokens bypass **CSE**.

$$\begin{aligned} \mathbf{x}_{i,0}^{(l+1)} &\leftarrow \mathbf{x}_{i,0}^{(l)} + \\ &\sum_h \mathbf{W}_O^{(l,h)} \mathbf{V}_{\text{CLS}}^{(l,h)} \text{Softmax} \left( \frac{1}{\sqrt{d_k}} \mathbf{K}_{\text{CLS}}^{(l,h)\top} \mathbf{R}_i \mathbf{q}_{i,0}^{(l,h)} \right) \\ \mathbf{V}_{\text{CLS}}^{(l,h)} &= \mathbf{W}_V^{(l,h)} [\{\mathbf{x}_{i,0}^{(l)}\}_{i=1}^m] = [\{\mathbf{v}_{i,0}^{(l,h)}\}_{i=1}^m] \\ \mathbf{K}_{\text{CLS}}^{(l,h)} &= \text{RoPE}(\mathbf{W}_K^{(l,h)} [\{\mathbf{x}_{i,0}^{(l)}\}_{i=1}^m]) = [\{\mathbf{R}_i \mathbf{k}_{i,0}^{(l,h)}\}_{i=1}^m] \end{aligned} \quad (2)$$

where  $\mathbf{q}_{i,0}^{(l,h)} = \mathbf{W}_Q^{(l,h)} \mathbf{x}_{i,0}^{(l)}$  is the query vector of the **[CLS]** token in  $\mathcal{X}_i$ ,  $\mathbf{W}_O^{(l,h)}, \mathbf{W}_Q^{(l,h)}, \mathbf{W}_K^{(l,h)}, \mathbf{W}_V^{(l,h)} \in \mathbb{R}^{d_{\text{model}} \times d_k}$  are the head-specific projection matrices in the multi-head attention of **CSE**, and  $\mathbf{R}_i$  is the rotary matrix for position  $i$ .

Now, all the **[CLS]** tokens carry information from all tokens across the event stream. When the contextualized embeddings subsequently pass through **SWE** in the next NEST layer, the non-**[CLS]** tokens in  $\mathcal{X}_i$  receive information about all the other multisets through  $\mathbf{x}_{i,0}$ . Indirect cross-set token interactions are achieved through the dual-level contextualization across layers. More importantly, the proposed architecture enforces an inductive bias whereby  $\{\mathbf{x}_{i,0}\}_{i=1}^m$ , the **[CLS]** token embeddings, serve as the representations of their corresponding multisets and can be directly used for downstream tasks.

### 3.4 Masked Set Modeling

The hierarchical architecture design provides a foundation for modeling the sequence of sets. To fully leverage structure in the data, we develop a Masked Set Modeling (MSM) procedure in addition to the standard MLM pretraining.

Let  $\mathcal{V}$  be the tokenizer vocabulary. Each multiset  $\mathcal{X}_i$  can be viewed as a random draw from a multinomial distribution  $M_{|\mathcal{V}|}(n; \{\pi_\theta(v)\}_{v=0 \dots |\mathcal{V}|-1})$  parameterized based on the context in the event trajectory  $\mathcal{H}_m$ . We derive the MSM objective from the likelihood function and reformulate it in terms of the Kullback-Leibler (KL) divergence; see Appendix A for full details of the derivation.

MSM is applied in parallel to the standard MLM objective. Each multiset  $\mathcal{X}_i$  has a 40% chance of being masked, where all tokens, including **[PAD]** but excluding **[CLS]**, are replaced with **[MASK]**. Then, we use the final contextualized embedding of **[CLS]** from  $\mathcal{X}_i$  to predict the masked tokens with a nonlinear projection head. Similar to MLM [5], the task is applied to the masked multisets.

**Definition 1.** The MSM loss is a distributional matching between the predicted token distribution  $\pi_\theta \in \Delta^{|\mathcal{V}|}$  and the observed token distribution  $p$  within each multiset.  $\Delta^{|\mathcal{V}|}$  is the probability simplex,

and  $p$  is empirically obtained from frequency counts of tokens in each multiset.

$$\mathcal{L}_{\text{MSM}} = D_{\text{KL}}(p \parallel \pi_{\theta})$$

$$\pi_{\theta} = \text{MLP}(\mathbf{x}_{i,0}), \text{ where } \text{MLP} : \mathbb{R}^{d_{\text{model}}} \rightarrow \Delta^{|\mathcal{V}|}$$

**Proposition 1** (Fast Soft Support Matching under KL Gradient Update). *For each  $\mathcal{X}_i$ , the support of  $p$  is*

$$\mathcal{S}_i := \{v \in \mathcal{V} : p(v) > 0\},$$

*and let  $\pi_{\theta}^{(\tau)}$ , indexed by time step  $\tau$ , evolve under the gradient update with learning rate  $\beta$ :*

$$d\pi_{\theta} = -\tau\beta \cdot \nabla_{\pi_{\theta}} D_{\text{KL}}(p \parallel \pi_{\theta}), \quad \pi_{\theta} \in \Delta^{|\mathcal{V}|}. \quad (3)$$

*Then, for any  $v \in \mathcal{S}_i$ ,  $\pi_{\theta}^{(\tau)}(v)$  increases whenever  $\pi_{\theta}^{(\tau)}(v) < p(v)$ . Probability mass is transferred from indices  $v \notin \mathcal{S}_i$  to indices  $v \in \mathcal{S}_i$ .*

In most cases, each token (except [PAD]) appears at most once in a multiset. In an ideal setting, a padding-free multiset and a randomly initialized uniform  $\pi_{\theta}$ , the loss satisfies  $\mathcal{L}_{\text{MSM}} \approx \log(|\mathcal{V}|/n)$ . Using Definition 1, we perform gradient analyses and establish Proposition 1. See Appendix A for detailed derivation.

The self-supervised objective in MSM encourages the [CLS] token representations to capture the support of the empirical token distribution of each multiset, thereby ensuring the effectiveness of using the [CLS] embeddings  $\{\mathbf{x}_{i,0}\}$  for downstream tasks. No post-hoc set-level pooling is required; however, pooling of  $\{\mathbf{x}_{i,0}\}$  remains necessary for sequence-level downstream tasks.

### 3.5 Pretraining Procedure

**MSM’s Complementarity with MLM.** MLM encourages fine-grained token-level contextualization through the SWE, learning local co-occurrence patterns within each multiset. MSM encourages holistic set-level summarization, learning to compress an entire multiset into its [CLS] embedding. In practice, both objectives are computed in parallel with separate masking operations: 20% of tokens undergo standard MLM masking, while 40% of multisets undergo complete MSM masking. The two losses are combined as the overall optimization objective. A.1 provides a memory-efficient implementation that incorporates mixed precision and multitask gradient accumulation.

**Intuition and Design Choices.** While MLM operates at the token level, predicting individual masked tokens from the surrounding context, MSM operates at the set level, requiring the [CLS] representation to encode sufficient information to reconstruct the *entire* token distribution of the masked multiset. We adopt a fully masking strategy: all non-special tokens in selected multisets are replaced with [MASK] tokens, preventing information leakage from the MLM protocol [5, 23].

For a given multiset, as no within-set signal remains, MSM forces the [CLS] token to aggregate cross-set contextual information across the sequence through the CSE and infer the within-set information. Proposition 1 explains why this objective is effective: under KL gradient flow, the model first learns to identify which tokens belong to each set (support matching) before refining their relative frequencies.

**Set-based validation criteria.** We replace commonly used token-level metrics, such as MLM loss and token-level top- $k$  accuracy for masked token prediction, with set-based metrics, specifically Recall@ $K$  and NDCG@ $K$ , computed on randomly masked multisets for evaluation and early stopping. Additional details are provided in Appendix C.

## 4 Experiments

### 4.1 Computing efficiency

We compare NEST’s computing efficiency with commonly used standard Transformer architectures. For fairness, these counterparts are also updated using the modern recipe [36]. Table 1 provides the benchmark results of models’ computing efficiency on randomly generated batches of SeqSet data. We use the same set of architectural hyperparameters for all tested models:  $L = 6$ ,  $d_{\text{model}} = 768$ ,  $d_h = 2048$ ,  $n_{\text{heads}} = 12$ ,  $d_k = 64$ ,  $|\mathcal{V}| = 45000$ , batch size of 8 and context size of 2048 ( $n = 32$ ,  $m = 64$ ).

All metrics are normalized at the token level. Despite having more parameters, NEST requires fewer FLOPs/token and achieves higher throughputs. NEST is significantly more computationally efficient than BERT and Longformer [1]. In particular, compared to BERT, NEST achieves an 18.2% reduction in FLOPs/token and an approximately 55.7% increase in throughput. Eventually, NEST achieves lower GPU memory footprint (see in Table B.1) and faster training speeds despite a higher parameter count.

Table 1: Comparing different Transformers’ MLM pretraining efficiency and benchmarking the efficiency on a single NVIDIA H200 GPU.

model	attn mem. complexity	GFLOPs/token ( $\downarrow$ )	K tokens/sec ( $\uparrow$ )
BERT	$O(N^2)$	0.192	$26.49 \pm 1.47$
Longformer	$O(nN + mN)$	0.172	$31.37 \pm 2.09$
NEST	$O(nN + m^2)$	<b>0.157</b>	<b><math>41.26 \pm 1.60</math></b>
$\text{BERT}_{\text{MEA}}$	$O(N) \sim O(N^2)$	0.192	$30.20 \pm 1.63$
$\text{NEST}_{\text{MEA}}$	$O(N) \sim O(nN + m^2)$	<b>0.157</b>	<b><math>41.35 \pm 2.26</math></b>

Memory-Efficient Attention (MEA) reduces memory usage and improves runtime through optimized memory management while preserving the same FLOPs as standard attention [26]. We compare an MEA-enhanced BERT with NEST. Although MEA substantially improves BERT, NEST still outperforms the enhanced variant. In contrast, MEA has negligible impact on NEST, as NEST’s effective context window is hierarchically composed of smaller windows. We do not apply MEA to Longformer, as its sparse sliding-window attention is structurally incompatible and difficult to adapt MEA.

## 4.2 Real-world Datasets

To ensure the reproducibility of our study, we conduct experiments on three real-world datasets, including proprietary EHR data from our institution and two publicly available datasets: MIMIC-IV-hosp and Instacart. Table 2 summarizes dataset statistics along with NEST pretraining performance.  $\text{MSM}_0$  is the estimated loss for random initialized model using  $\log(|\mathcal{V}|/n)$  provided in Section 3.4. The lower loss values suggest that clinical dynamics are easier to learn than consumer behavior.

Table 2: SeqSet datasets’ statistics and NEST validation losses after 20 epochs of pretraining.

Dataset	#subject	#msets	#tokens	MLM	MSM/MSM <sub>0</sub>
Instacart	206K	3.42M	33.8M	6.27	1.51/7.25
Proprietary EHR	500K	7.34M	70.9M	2.52	0.31/6.15
MIMIC-IV hosp	223K	546K	122M	2.40	0.50/3.68

### 4.2.1 Instacart

This dataset is open sourced by Instacart<sup>1</sup>. The dataset consists of online grocery transactions used to develop model for Next Basket Recommendation (NBR). Orders are treated as baskets containing unordered and equally important items [19].

### 4.2.2 Proprietary institutional EHR

We developed an ETL pipeline that transforms heterogeneous tables from our institutional EHR database into a unified event-stream format. We collected medical event stream data from approximately 0.5M patients born between 1999 and 2024 and filtered events occurring between ages 0 and 18. Modeling the long-term patient timelines, we ignore the order of events within each encounter. We assign patients born on the 17th–24th of each month to the test set and the remainder to the training and validation splits.

<sup>1</sup>While the official source is no longer directly hosted, a copy of the dataset is available on Kaggle: *instacart-online-grocery-basket-analysis-dataset*.

#### 4.2.3 MIMIC-IV hosp

MIMIC-IV is a publicly dataset comprising de-identified electronic health records from Beth Israel Deaconess Medical Center [13]. We use version 3.1, which spans admissions from 2008 to 2022. We extract data from the `hosp` module across six source tables: `admissions`, `diagnoses_icd`, `procedures_icd`, `labevents`, `emar`, and `prescriptions`. The processed dataset contains 546K hospital admissions from 223K patients. We adopt the ETHOS’s [30] tokenization protocol with slight adjustments for the MIMIC-IV clinical event streams. See more details in Appendix D.2.

#### 4.3 Instacart NBR

Given a sequence of baskets  $\mathcal{H}_m = \{(\mathcal{X}_i, t_i)\}_{i=1}^m$  that a user has purchased in the past, the goal of a NBR system is to generate the basket of items  $\mathcal{X}_{m+1}$  that the user would like to purchase next. The items in the basket have no temporal order and are equally important. Various methods have been proposed for NBR in e-commerce shopping [8, 34, 9, 18].

NEST is directly applicable to the NBR. Following BTBR [18] and BERT4Rec [10], we rely solely on self-supervised pre-training and apply the model directly to NBR with no additional fine-tuning. After pretraining the model on user shopping histories, we adopt the inference protocol defined in BTBR [18], which adapts BERT-based model like BERT4Rec [34] for NBR. Specifically, a query basket,  $\mathcal{X}_{m+1} = \{[\text{MASK}]\}$ , is appended to the purchasing history  $\mathcal{H}_m$ , and the predicted future basket  $\hat{\mathcal{X}}_{m+1}$  is then formed by choosing the top- $k$  items with the highest logits produced at the masking token.

We use two commonly used metrics to compare NEST against other approaches: Recall@10 and NDCG@10 (see Appendix C for detailed formulas). Both evaluate the quality of the recommended basket at a fixed size of 10.

Table 3: Compare various methods for NBR. Bold indicates the highest value, and \* denotes the second-highest.

Model	Recall@10	NDCG@10
Sets2Sets [8]	21.2	19.2
TIFUKNN [9]	<b>36.0</b>	<b>37.2</b>
BERT4Rec [34]	25.3	29.9
NEST <sub>MLM-only</sub>	28.1*	34.9*
NEST <sub>SoftCLT</sub>	25.6	32.6
NEST	26.2	32.6

In NEST<sub>SoftCLT</sub>, we adopt SoftCLT [17] as a plug-and-play secondary loss alongside MLM. The pretrain procedure is similar to unsupervised SimCSE with MLM [6], detailed in the Appendix E. Although achieving comparable (or slightly lower) performance than MSM, it has many moving parts and tuning parameters.

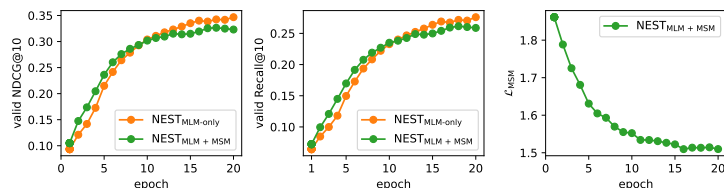


Figure 4: NEST validation NBR performance during the training. Set prediction is challenging in this dataset, where the validation MSM loss converges at 1.5.

One key observation is that when both architectures are pretrained with MLM using the same optimizer and learning-rate setup, the flat Transformer (BERT4Rec) shows degradation in validation NBR performance as training progresses, while NEST’s performance remains stable over a longer time horizon, independent of whether set-representation constraints are applied.

Table 4: BERT4Rec vs NEST on masked token prediction.

Model	Top-1 Acc	Top-10 Acc
BERT4Rec	14.5	34.5
NEST <sub>MLM-only</sub>	17.8 (↑ 23%)	36.5 (↑ 5.8%)
NEST <sub>SoftCLT</sub>	17.4	34.3
NEST	<b>17.8 (↑ 23%)</b>	<b>36.8 (↑ 6.7%)</b>

#### 4.4 MIMIC-IV

We compare NEST against three baselines: Hi-BEHRT [21], CORE-BEHRT [23], and GT-BEHRT [24], all built with matched architecture hyperparameters for fair comparison. We originally planned to include HEART [11], but its  $O(N^2)$  pairwise edge embeddings caused frequent OOM failures and NaN losses during training, so we excluded it from the comparison. The evaluation covers six downstream tasks: inpatient mortality prediction (prevalence 2.2%), 30-day readmission (33.9%), prolonged length of stay (17.9%), ICD chapter classification, and ICD category multi-label classification. Detailed task definitions are provided in Appendix D.3.

Table 5: MIMIC-IV finetuned downstream performance.

(a) AUROC

Model	Mortality	Readmission	Prolonged LOS	ICD Chapter	ICD Category
Hi-BEHRT	87.6	61.9	73.6	91.4	87.5
CORE-BEHRT	92.2	70.7	86.2	93.2	92.2
GT-BEHRT	93.8	71.1	85.0	91.6	92.0
NEST <sub>MLM-only</sub>	95.2	72.4	88.8	95.0	92.6
NEST	<b>95.4</b>	<b>72.4</b>	<b>88.9</b>	<b>95.2</b>	<b>93.7</b>

(b) AP

Model	Mortality	Readmission	Prolonged LOS	ICD Chapter	ICD Category
Hi-BEHRT	33.5	45.6	36.9	43.7	10.1
CORE-BEHRT	43.8	55.8	58.9	57.0	15.7
GT-BEHRT	42.1	56.4	56.0	55.4	12.5
NEST <sub>MLM-only</sub>	51.1	58.4	64.0	72.4	16.4
NEST	<b>52.3</b>	<b>58.8</b>	<b>64.3</b>	<b>72.8</b>	<b>16.8</b>

#### 4.5 FM for proprietary EHR data

In downstream tasks, we obtain patient representation by encoding the truncated prefix  $\mathcal{H}_{\leq a}$  to predict targeted clinical events occurring after the discharge time  $t_a$ . This calculation examine FMs' performances on preventive risk prediction.

We curated three binary classification cohorts: (i) Home Health Care 30-day readmission (20%), (ii) Autism Spectrum Disorder (ASD) (3%), and (iii) Recurrent Acute Otitis Media (rAOM) (22%). More details of the data pipeline and cohorts' clinical significance are provided in Appendix D.4. These tasks focus on pediatric cohorts, aiming to support in-house clinical decision-making for preventive care. We benchmark our model's performance on these tasks against count-based LightGBM [16, 38] and CORE-BEHRT [23].

In Table 6, for foundation models, we report performance under both nonlinear probing (with the backbone frozen) and full fine-tuning (with the backbone adapted to the downstream task).

Table 6: Performance on downstream tasks.

Model	rAOM		ASD		30d Readmit	
	AUROC	AP	AUROC	AP	AUROC	AP
LightGBM	71.7	40.1	73.6	6.0	73.8	46.6
CORE-BEHRT <sub>pb</sub>	72.1	39.6	70.3	9.8	73.8	46.8
CORE-BEHRT <sub>ft</sub>	73.0	<b>43.9</b>	73.8	10.2	73.8	46.8
NEST <sub>pb</sub>	73.7	42.6	71.1	7.6	73.4	45.7
NEST <sub>ft</sub>	<b>73.8</b>	43.2	<b>74.2</b>	<b>10.9</b>	<b>74.1</b>	<b>47.5</b>

## 5 Ablation Study: What Does MSM Provide?

We ablate the MSM objective to understand its contribution to NEST pretraining. Specifically, we ask: (1) Does MSM improve set-level prediction? (2) Does the learned representation transfer beyond the task-specific head?

We pretrain three small (3-layer) NEST variants on the proprietary EHR data for 10 epochs: MSM-only, MLM-only, and MLM+MSM. To evaluate whether set-level knowledge resides in the encoder rather than the MSM task head, we measure set prediction performance using a weight-tied linear layer [25] instead of the MSM task head used in the pretraining.

Table 7: Set prediction performance (Recall@10, NDCG@10) on randomly masked encounters.

Model	Recall@10	NDCG@10
MSM-only	<0.01	<0.01
MLM-only	47.6	51.6
MLM+MSM	<b>48.9</b> (↑2.7%)	<b>54.9</b> (↑6.4%)

MSM-only pretraining fails entirely: the task head learns to predict sets, but the encoder representations do not transfer. MLM-only provides a strong baseline, but combining MLM with MSM yields consistent improvements across both metrics. This confirms that the two objectives are complementary: MLM drives token-level contextualization, while MSM encourages the [CLS] embedding to capture set-level information in a transferable manner.

## 6 Conclusion

We introduced NEST, a hierarchical Transformer for event streams that can be structured as SeqSet. By employing hierarchical Transformer layers with SWE and CSE, NEST preserves multiset boundaries and induces structured sparsity, achieving significantly higher throughput than standard BERT-style baselines. Masked Set Modeling provides explicit set-level supervision, yielding directly usable [CLS] embeddings without post-hoc pooling. Experiments on MIMIC-IV, proprietary EHR, and Instacart demonstrate improvements in both efficiency and downstream tasks.

## Software and Data

We will make the code repository publicly available upon acceptance. MIMIC-IV and Instacart are public datasets, but the institutional proprietary EHR data are not publicly available due to privacy but are available from the corresponding author on reasonable request.

## Impact Statement

This paper presents work to advance the field of Machine Learning. There are many potential societal consequences of our work, none which we feel must be specifically highlighted here.

## References

- [1] Iz Beltagy, Matthew E Peters, and Arman Cohan. Longformer: The long-document transformer. *arXiv preprint arXiv:2004.05150*, 2020.
- [2] Ilias Chalkidis, Ion Androutsopoulos, and Nikolaos Aletras. Neural legal judgment prediction in english. In *Proceedings of the 57th Annual Meeting of the Association for Computational Linguistics*. Association for Computational Linguistics, 2019.
- [3] Ilias Chalkidis, Xiang Dai, Manos Fergadiotis, Prodromos Malakasiotis, and Desmond Elliott. An exploration of hierarchical attention transformers for efficient long document classification. *arXiv preprint arXiv:2210.05529*, 2022.
- [4] Yung-Sung Chuang, Rumen Dangovski, Hongyin Luo, Yang Zhang, Shiyu Chang, Marin Soljačić, Shang-Wen Li, Scott Yih, Yoon Kim, and James Glass. Diffcse: Difference-based contrastive learning for sentence embeddings. In *Proceedings of the 2022 Conference of the North American Chapter of the Association for Computational Linguistics: Human Language Technologies*, pages 4207–4218, 2022.
- [5] Jacob Devlin, Ming-Wei Chang, Kenton Lee, and Kristina Toutanova. Bert: Pre-training of deep bidirectional transformers for language understanding. In *Proceedings of the 2019 conference of the North American chapter of the association for computational linguistics: human language technologies, volume 1 (long and short papers)*, pages 4171–4186, 2019.
- [6] Tianyu Gao, Xingcheng Yao, and Danqi Chen. Simcse: Simple contrastive learning of sentence embeddings. In *Proceedings of the 2021 Conference on Empirical Methods in Natural Language Processing*, page 6894. Association for Computational Linguistics, 2021.
- [7] Haoyu He, Markus Flicke, Jan Buchmann, Iryna Gurevych, and Andreas Geiger. Hdt: Hierarchical document transformer. *arXiv preprint arXiv:2407.08330*, 2024.
- [8] Haoji Hu and Xiangnan He. Sets2sets: Learning from sequential sets with neural networks. In *Proceedings of the 25th ACM SIGKDD International Conference on Knowledge Discovery & Data Mining*, pages 1491–1499, 2019.
- [9] Haoji Hu, Xiangnan He, Jinyang Gao, and Zhi-Li Zhang. Modeling personalized item frequency information for next-basket recommendation. In *Proceedings of the 43rd international ACM SIGIR conference on research and development in information retrieval*, pages 1071–1080, 2020.
- [10] Sihao Hu, Zhen Zhang, Bingqiao Luo, Shengliang Lu, Bingsheng He, and Ling Liu. Bert4eth: A pre-trained transformer for ethereum fraud detection. In *Proceedings of the ACM Web Conference 2023*, pages 2189–2197, 2023.
- [11] Tingyi Huang, Shreya Saini, Aditya Nagarajan, Young-Rock Chung, Shayok Bhattacharyya, and Tengfei Ma. Heart: Learning better representation of ehr data with a heterogeneous relation-aware transformer. *Journal of Biomedical Informatics*, 152:104623, 2024.
- [12] Hyewon Jeong, Nassim Oufattolle, Matthew Mcdermott, Aparna Balagopalan, Bryan Jangeesingh, Marzyeh Ghassemi, and Collin Stultz. Event-based contrastive learning for medical time series. *arXiv preprint arXiv:2312.10308*, 2023.
- [13] Alistair EW Johnson, Lucas Bulgarelli, Lu Shen, Alvin Gayles, Ayad Shammout, Steven Horng, Tom J Pollard, Sicheng Hao, Benjamin Moody, Brian Gow, et al. Mimic-iv, a freely accessible electronic health record dataset. *Scientific data*, 10(1):1, 2023.
- [14] Wang-Cheng Kang and Julian McAuley. Self-attentive sequential recommendation. In *2018 IEEE international conference on data mining (ICDM)*, pages 197–206. IEEE, 2018.
- [15] Seyed Mehran Kazemi, Rishab Goel, Sepehr Eghbali, Janahan Ramanan, Jaspreet Sahota, Sanjay Thakur, Stella Wu, Cathal Smyth, Pascal Poupart, and Marcus Brubaker. Time2vec: Learning a vector representation of time. *arXiv preprint arXiv:1907.05321*, 2019.
- [16] Guolin Ke, Qi Meng, Thomas Finley, Taifeng Wang, Wei Chen, Weidong Ma, Qiwei Ye, and Tie-Yan Liu. Lightgbm: A highly efficient gradient boosting decision tree. *Advances in neural information processing systems*, 30, 2017.
- [17] Seunghan Lee, Taeyoung Park, and Kibok Lee. Soft contrastive learning for time series. 2024. Publisher Copyright: © 2024 12th International Conference on Learning Representations, ICLR 2024. All rights reserved.; 12th International Conference on Learning Representations, ICLR 2024 ; Conference date: 07-05-2024 Through 11-05-2024.

[18] Ming Li, Mozhdeh Ariannezhad, Andrew Yates, and Maarten De Rijke. Masked and swapped sequence modeling for next novel basket recommendation in grocery shopping. In *Proceedings of the 17th ACM Conference on Recommender Systems*, pages 35–46, 2023.

[19] Ming Li, Sami Jullien, Mozhdeh Ariannezhad, and Maarten De Rijke. A next basket recommendation reality check. *ACM Transactions on Information Systems*, 41(4):1–29, 2023.

[20] Yikuan Li, Shishir Rao, José Roberto Ayala Solares, Abdelaali Hassaine, Rema Ramakrishnan, Dexter Canoy, Yajie Zhu, Kazem Rahimi, and Gholamreza Salimi-Khorshidi. Behrt: transformer for electronic health records. *Scientific reports*, 10(1):7155, 2020.

[21] Yikuan Li, Mohammad Mamouei, Gholamreza Salimi-Khorshidi, Shishir Rao, Abdelaali Hassaine, Dexter Canoy, Thomas Lukasiewicz, and Kazem Rahimi. Hi-behrt: hierarchical transformer-based model for accurate prediction of clinical events using multimodal longitudinal electronic health records. *IEEE journal of biomedical and health informatics*, 27(2):1106–1117, 2022.

[22] Matthew McDermott, Bret Nestor, Peniel Argaw, and Isaac S Kohane. Event stream gpt: a data pre-processing and modeling library for generative, pre-trained transformers over continuous-time sequences of complex events. *Advances in Neural Information Processing Systems*, 36:24322–24334, 2023.

[23] Mikkel Odgaard, Kiril Vadimovic Klein, Sanne Møller Thysen, Espen Jimenez-Solem, Martin Sillesen, and Mads Nielsen. Core-behrt: A carefully optimized and rigorously evaluated behrt. *arXiv preprint arXiv:2404.15201*, 2024.

[24] Raphael Poulain and Rahmatollah Beheshti. Graph transformers on EHRs: Better representation improves downstream performance. In *The Twelfth International Conference on Learning Representations*, 2024. URL <https://openreview.net/forum?id=pe0Vdv7rsL>.

[25] Ofir Press and Lior Wolf. Using the output embedding to improve language models. In *Proceedings of the 15th Conference of the European Chapter of the Association for Computational Linguistics: Volume 2, Short Papers*, pages 157–163, 2017.

[26] Markus N. Rabe and Charles Staats. Self-attention does not need  $\mathcal{O}(n^2)$  memory. *arXiv preprint arXiv:2112.05682*, 2021.

[27] Alec Radford, Karthik Narasimhan, Tim Salimans, Ilya Sutskever, et al. Improving language understanding by generative pre-training. 2018.

[28] Laila Rasmy, Yang Xiang, Ziqian Xie, Cui Tao, and Degui Zhi. Med-bert: pretrained contextualized embeddings on large-scale structured electronic health records for disease prediction. *NPJ digital medicine*, 4(1):86, 2021.

[29] Nils Reimers and Iryna Gurevych. Sentence-bert: Sentence embeddings using siamese bert-networks. In *Proceedings of the 2019 Conference on Empirical Methods in Natural Language Processing and the 9th International Joint Conference on Natural Language Processing (EMNLP-IJCNLP)*, pages 3982–3992, 2019.

[30] Paweł Renc, Yugang Jia, Anthony E Samir, Jarosław Was, Quanzheng Li, David W Bates, and Arkadiusz Sitek. Zero shot health trajectory prediction using transformer. *NPJ digital medicine*, 7(1):256, 2024.

[31] Noam Shazeer. Glu variants improve transformer. *arXiv preprint arXiv:2002.05202*, 2020.

[32] Ethan Steinberg, Jason Fries, Yizhe Xu, and Nigam Shah. Motor: A time-to-event foundation model for structured medical records. *arXiv preprint arXiv:2301.03150*, 2023.

[33] Jianlin Su, Murtadha Ahmed, Yu Lu, Shengfeng Pan, Wen Bo, and Yunfeng Liu. Roformer: Enhanced transformer with rotary position embedding. *Neurocomputing*, 568:127063, 2024.

[34] Fei Sun, Jun Liu, Jian Wu, Changhua Pei, Xiao Lin, Wenwu Ou, and Peng Jiang. Bert4rec: Sequential recommendation with bidirectional encoder representations from transformer. In *Proceedings of the 28th ACM international conference on information and knowledge management*, pages 1441–1450, 2019.

[35] Ashish Vaswani, Noam Shazeer, Niki Parmar, Jakob Uszkoreit, Llion Jones, Aidan N Gomez, Łukasz Kaiser, and Illia Polosukhin. Attention is all you need. *Advances in neural information processing systems*, 30, 2017.

- [36] Benjamin Warner, Antoine Chaffin, Benjamin Clavié, Orion Weller, Oskar Hallström, Said Taghadjouini, Alexis Gallagher, Raja Biswas, Faisal Ladhak, Tom Aarsen, et al. Smarter, better, faster, longer: A modern bidirectional encoder for fast, memory efficient, and long context finetuning and inference. In *Proceedings of the 63rd Annual Meeting of the Association for Computational Linguistics (Volume 1: Long Papers)*, pages 2526–2547, 2025.
- [37] Sean Welleck, Zixin Yao, Yu Gai, Jialin Mao, Zheng Zhang, and Kyunghyun Cho. Loss functions for multiset prediction. *Advances in Neural Information Processing Systems*, 31, 2018.
- [38] Michael Wornow, Rahul Thapa, Ethan Steinberg, Jason Fries, and Nigam Shah. Ehrshot: An ehr benchmark for few-shot evaluation of foundation models. *Advances in Neural Information Processing Systems*, 36: 67125–67137, 2023.
- [39] Ruibin Xiong, Yunchang Yang, Di He, Kai Zheng, Shuxin Zheng, Chen Xing, Huishuai Zhang, Yanyan Lan, Liwei Wang, and Tieyan Liu. On layer normalization in the transformer architecture. In *International conference on machine learning*, pages 10524–10533. PMLR, 2020.
- [40] Zichao Yang, Diyi Yang, Chris Dyer, Xiaodong He, Alex Smola, and Eduard Hovy. Hierarchical attention networks for document classification. In *Proceedings of the 2016 conference of the North American chapter of the association for computational linguistics: human language technologies*, pages 1480–1489, 2016.
- [41] Manzil Zaheer, Guru Guruganesh, Kumar Avinava Dubey, Joshua Ainslie, Chris Alberti, Santiago Ontanon, Philip Pham, Anirudh Ravula, Qifan Wang, Li Yang, et al. Big bird: Transformers for longer sequences. *Advances in neural information processing systems*, 33:17283–17297, 2020.
- [42] Yan Zhang, Jonathon Hare, and Adam Prugel-Bennett. Deep set prediction networks. *Advances in Neural Information Processing Systems*, 32, 2019.

## A MSM

### A.1 Loss derivation

Let  $l(\theta; \mathcal{X}_i)$  be the multinomial log-likelihood of multiset  $\mathcal{X}_i$ . Let  $\triangleq$  denote “equal up to an additive constant”.

$$-l(\theta; \mathcal{X}_i) = -\log \left( \frac{n!}{n_0! n_1! \cdots n_{|\mathcal{V}|-1}!} \pi_\theta(0)^{n_0} \pi_\theta(1)^{n_1} \cdots \pi_\theta(|\mathcal{V}|-1)^{n_{|\mathcal{V}|-1}} \right) \quad (\text{A.1})$$

$$\triangleq - \sum_{v=0}^{|\mathcal{V}|-1} n_v \log \pi_\theta(v) \quad (\text{A.2})$$

$$\propto - \sum_{v=0}^{|\mathcal{V}|-1} \underbrace{\frac{n_v}{n}}_{p(v)} \log \pi_\theta(v) \quad (\text{A.3})$$

$$\triangleq \mathbb{E}_{v \sim p} \left[ \log \frac{p(v)}{\pi_\theta(v)} \right] \quad [\text{entropy } H(p) \text{ is constant w.r.t. } \theta] \quad (\text{A.4})$$

$$= D_{\text{KL}}(p \parallel \pi_\theta) \stackrel{\text{def}}{=} \mathcal{L}_{\text{MSM}} \quad (\text{A.5})$$

### A.2 Proposition derivation

**Gradient analysis of MSM for Proposition 1.** Let’s consider an arbitrary multiset  $\mathcal{X}_i$  with observed token distribution  $p$  and predicted distribution  $\pi_\theta$  that is **uniformly initialized**. There are  $k$  [PAD] tokens in  $\mathcal{X}_i$ , where  $k \geq 0$ . Also, assume all non-[PAD] appears once in the multiset.

Let  $o_v$  be the logits of token  $v$  from the vocabulary  $\mathcal{V}$  in the MSM task.  $|\mathcal{X}_i| = n \ll |\mathcal{V}|$ . Now, we can calculate the gradient:

$$\frac{\partial D_{\text{KL}}}{\partial o_v} = \sum_{u \in \mathcal{V}} \frac{\partial D_{\text{KL}}}{\partial \log \pi_\theta(u)} \cdot \frac{\partial \log \pi_\theta(u)}{\partial o_v} = \sum_u -p(u)(\delta_{vu} - \pi_\theta(v)) = \pi_\theta(v) - p(v) \quad (\text{A.6})$$

Let  $\alpha = \mathbb{I}[v \neq \text{[PAD]}]$ :

- if token  $v \in \mathcal{X}_i$ ,  $p(v) = \alpha \cdot \frac{1}{n} + (1 - \alpha) \cdot \frac{k}{n}$ , then  $\pi_\theta(v) \ll p(v) \Rightarrow$  large negative gradient that pushes  $o_v$  to be large in gradient descent
- if token  $v \notin \mathcal{X}_i$ ,  $p(v) = 0$ , then  $\pi_\theta(v) > p = 0 \Rightarrow$  small positive gradient that pushes  $o_v$  to be small in gradient descent

Intuitively, the probability mass rapidly moves onto the multiset  $\mathcal{X}_i$ ’s support,  $\mathcal{S}_i = \{v : v \in \mathcal{X}_i\} = \{v \in \mathcal{V} : p(v) > 0\}$ .

### Decompose $D_{\text{KL}}$ for Proposition 1.

$$D_{\text{KL}}(p \parallel \pi_\theta) = \sum_{v \in \mathcal{V}} p(v) \log \frac{p(v)}{\pi_\theta(v)} = \frac{k}{n} \log \left( \frac{k/n}{\pi_\theta(\text{[PAD]})} \right) + \frac{1}{n} \sum_{\substack{v \neq \text{[PAD]} \\ v \in \mathcal{S}_i}} \log \left( \frac{1/n}{\pi_\theta(v)} \right) \quad (\text{A.7})$$

### A.3 Pretraining Procedure

We use automatic mixed precision (amp) and gradient accumulation to further improve memory and computing efficiency during the model pretraining. Algorithm A.1 is a single-sample, single-step illustration of the pretraining procedure.

---

**Algorithm A.1** NEST pretraining with amp and multitask gradient accumulation (a single-sample, single-step illustration)

---

**Initialize:** model NEST, optimizer  $\mathcal{O}$ , GradScaler  $\mathcal{S}$   
**Data Input:** masked event stream:  $\mathcal{H}_m^{(\text{MLM})}, \mathcal{H}_m^{(\text{MSM})}$

```

 $\mathcal{O}.\text{zero\_grad}()$ 
Pass 1: MLM
with autocast(fp16):
     $\text{out}_{\text{MLM}} \leftarrow \text{NEST}(\mathcal{H}_m^{(\text{MLM})})$ 
    get masked token logits  $\hat{o}_{\text{MLM}}$  and ground truths  $y_{\text{MLM}}$ 
     $\ell_1 \leftarrow \mathcal{L}_{\text{MLM}}(\hat{o}_{\text{MLM}}, y_{\text{MLM}})$  {CE for masked token prediction}
     $\mathcal{S}.\text{scale}(\ell_1).\text{backward}()$ 
    del  $\text{out}_{\text{MLM}}$ 
Pass 2: MSM
with autocast(fp16):
     $\text{out}_{\text{MSM}} \leftarrow \text{NEST}(\mathcal{H}_m^{(\text{MSM})})$ 
    get masked set logits  $\hat{o}_{\text{MSM}}$  and ground truths  $y_{\text{MSM}}$ 
     $\ell_2 \leftarrow \mathcal{L}_{\text{MSM}}(\hat{o}_{\text{MSM}}, y_{\text{MSM}})$  {KLDiv for masked multiset distribution prediction}
     $\mathcal{S}.\text{scale}(\ell_2).\text{backward}()$ 
     $\mathcal{S}.\text{step}(\mathcal{O})$ 
     $\mathcal{S}.\text{update}()$ 

```

---

## B Model Sizes

Table B.1: Model size and peak memory usage tested over 30 batches of randomly generate SeqSet data.  $L = 6, d_{\text{model}} = 768, d_h = 2048, n_{\text{heads}} = 12, d_k = 64, |\mathcal{V}| = 45000$ , batch size of 8 and context size of 2048 ( $n = 32, m = 64$ ).

Model	param. size (M)	avg peak mem. (GiB ↓)
BERT	77	41.6
Longformer	88	31.8
BERT <sub>MEA</sub>	77	24.7
NEST	120	23.9
NEST <sub>MEA</sub>	120	23.7

Longformer has higher parameter size than BERT, because it has an additional set of linear projections (Q, K, V) for global attention scores in each layer. NEST is the most parameterized since each layer is consist of two Transformer modules: SWE and CSE. MEA only replaces the standard scaled dot product for self-attention, so it does not change the parameter size.

## C Multiset Prediction

During pretraining, we employ a separate MSM task head for set prediction. However, this setup may overestimate representation quality, as set-level information can be largely absorbed by the MSM-task head while the FM backbone remains insufficiently optimized—in other words, the MSM-task head may perform most of the heavy lifting. To mitigate this issue, we adopt a more conservative strategy when evaluating FM representation quality by computing the missing tokens for a masked set without relying on the MSM head. Specifically, analogous to MLM, we use the shared output layer (tied with

the input embedding layer) to compute logits and select the top- $k$  candidates to form the predicted set.

As the predicted set is formed from the top- $k$  predicted token logits, we evaluate set prediction for both NBR and MSM using Recall@ $K$  and NDCG@ $K$  (normalized discounted cumulative gain for  $K$  predictions).

$$\text{Recall}@K(u) = \frac{|T_u \cap P_u|}{|T_u|} \quad (\text{C.1})$$

$$\text{NDCG}@K(u) = \frac{\sum_{k=1}^K p_k / \log_2(k+1)}{\sum_{k=1}^{\min(K, |T_u|)} 1 / \log_2(k+1)} \quad (\text{C.2})$$

where  $T_u$  and  $P_u$  are the ground truth set (which need not be in a size of  $K$ ) and predicted set with  $K$  recommended items for subject  $u$  and  $p_k = \mathbb{I}\{P_u^{(k)} \in T_u\}$ . Recall@ $K$  quantifies model's ability to find the relevant items, and NDCG@ $K$  measures model's ability to push all correct tokens to the front of the recalled tokens.

## D Real-world datasets

### D.1 Instacart

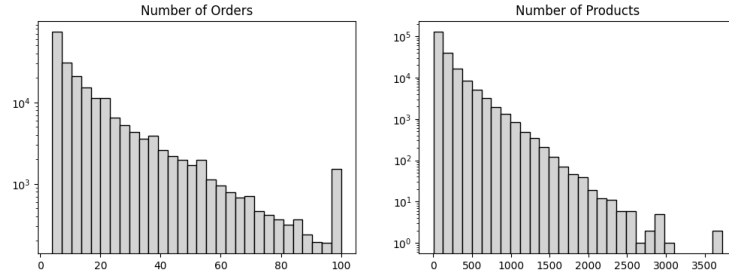


Figure D.1: Distributions for # multisets and # tokens per user.

### D.2 MIMIC-IV v3.1 - hosp

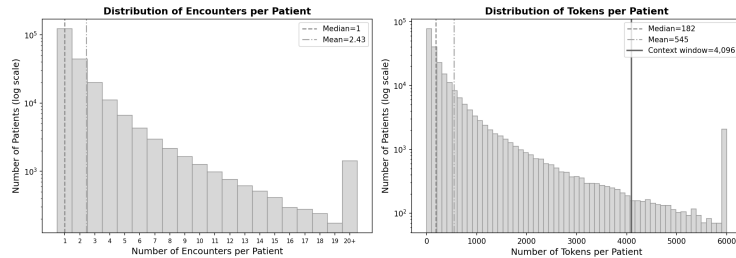


Figure D.2: Distributions for # multisets and # tokens per patient.

**Tokenization.** Following ETHOS [30], we construct four clinical event types with standardized medical codes:

- **Diagnoses (DX):** ICD-9-CM codes are converted to ICD-10-CM using CMS General Equivalence Mappings (GEM). When one ICD-9 maps to multiple ICD-10 codes, we select the shortest following ETHOS. Unmappable codes (marked NoDx in GEM) are excluded. Format: DX:{icd10}.
- **Procedures (PR):** ICD-9-PCS codes are converted to ICD-10-PCS with the same shortest-match strategy. Unmappable codes (NoPCS) are excluded. Format: PR:{icd10pcs}.

- **Medications (MED):** We extract administered medications from `emar` (filtering `event_txt='Administered'`). Drug names are mapped to ATC codes via a lookup table constructed from `prescriptions`: the GSN (Generic Sequence Number) field is mapped to ATC using external GSN-ATC mappings. Format: `MED:{atc}`.
- **Labs (LAB):** We select the 200 most frequent lab items, covering approximately 95% of all lab observations. Continuous values are discretized into deciles (Q1–Q10) using population-level quantile thresholds. Labs occurring within 24 hours before admission are also included. Format: `LAB:{itemid}_Q{1-10}`. This approach integrates numerical information into the modeling process.

**Temporal structure.** ETHOS flattens patient timelines into a 1D sequence using time-interval separator tokens. In contrast, NEST preserves the hierarchical multiset structure while retaining temporal ordering within each multiset. Each hospital admission forms a multiset, with events ordered internally by `time_offset_hours` relative to admission time. Diagnoses, which lack timestamps, are placed at offset  $-0.001h$  to ensure they appear first. Across admissions, `days_since_prior_admission` provides inter-admission temporal context for RoPE-based positional encoding in the CSE.

### D.3 Downstream Tasks

We evaluate NEST on six downstream tasks, covering clinical outcome prediction, diagnosis classification, and future event prediction. All tasks use patient-level 70/15/15 train/validation/test splits to prevent information leakage between patients.

**Prediction Mechanism.** For all downstream tasks, the pre-trained encoder processes the patient’s admission sequence and produces contextualized representations. Each segment is prepended with a `[CLS]` token. For classification, we extract the `[CLS]` representation from the last valid segment and pass it through a two-layer MLP (with GELU activation and dropout) to produce logits. Binary and multi-class tasks use cross-entropy loss; multi-label tasks (ICD category) use binary cross-entropy loss.

#### Task Definitions.

- **Inpatient Mortality.** Binary classification predicting whether a patient dies during the hospital stay. Following prior work, we use only data from the first 24 hours after admission to enable early prediction while preventing data leakage. Diagnoses from the target admission are excluded. Evaluated using AUROC and AUPRC.
- **30-Day Readmission.** Binary classification predicting whether a patient is readmitted within 30 days after discharge. Patients who die during hospitalization or have no subsequent admission record are excluded from this task. Prediction is made at discharge time using full admission data (including diagnoses). Evaluated using AUROC and AUPRC.
- **Prolonged Length of Stay.** Binary classification predicting whether the hospital stay exceeds 7 days. We use only data from the first 48 hours after admission for prediction. Diagnoses from the target admission are excluded to prevent leakage. Evaluated using AUROC and AUPRC.
- **ICD Chapter Classification.** Multi-class classification predicting the primary diagnosis ICD chapter (based on the `seq_num=1` diagnosis code). ICD-10-CM codes are mapped to 22 chapters; ICD-9-CM codes are mapped to corresponding chapter equivalents. Prediction is made at discharge, with target admission diagnoses excluded. Evaluated using macro-averaged AUROC and AUPRC.
- **ICD Category Multi-label Classification.** Multi-label classification predicting all 3-character ICD categories present in the admission. We retain categories appearing in at least 100 admissions. Labels are represented as multi-hot vectors over the category vocabulary. Prediction is made at discharge with target diagnoses excluded. Evaluated using macro-averaged AUROC and AUPRC.

**Data Leakage Prevention.** For mortality and prolonged LoS tasks, we apply temporal truncation to limit input data to the first 24h and 48h after admission, respectively. For all classification tasks

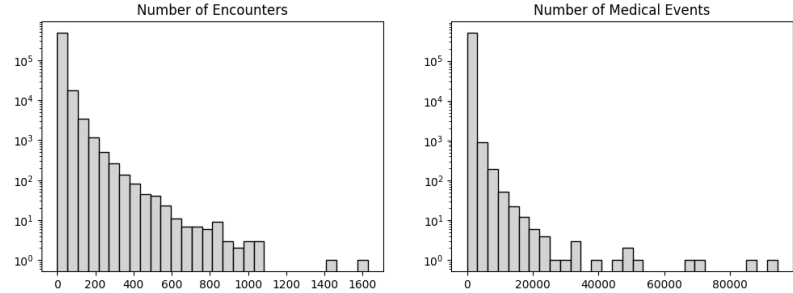


Figure D.3: Distributions for # multisets and # tokens per patient.

except readmission, we exclude diagnosis codes (DX:\*) from the target admission to prevent trivial prediction.

**Evaluation Metrics.** Binary classification tasks use AUROC and AUPRC as primary metrics. Multi-class and multi-label tasks use macro-averaged AUROC and AUPRC, computed via one-vs-rest per class then unweighted averaging.

Table D.1: Summary of downstream task configurations.

Task	Type	Prediction Time	Exclude DX	Primary Metric
Mortality	Binary	Admission + 24h	Yes	AUROC / AUPRC
30-Day Readmission	Binary	Discharge	No	AUROC / AUPRC
Prolonged LoS	Binary	Admission + 48h	Yes	AUROC / AUPRC
ICD Chapter	Multi-class	Discharge	Yes	Macro AUROC / AUPRC
ICD Category	Multi-label	Discharge	Yes	Macro AUROC / AUPRC

## D.4 Proprietary EHR

The train-test split in the downstream task cohorts follows the deterministic birth-date-based split of the pretrain data. Patients born on the 17th–24th of each month are assigned to the test set and the remainder to the training set.

### D.4.1 ETL pipeline

We implemented an ETL data processing pipeline to extract multi-source, heterogeneous EHR tables from a clinical Oracle database conforming to the PCORnet Common Data Model (CDM). The ETL process is organized around patients’ longitudinal clinical histories and retrieves structured clinical events from patient demographics, diagnoses, procedures, laboratory measurements, medication administrations and prescriptions, vital signs, and immunizations. All records are joined, filtered, and indexed at both the patient and encounter levels. Clinical records from different domains are subsequently normalized into a shared base schema, consisting of standardized patient and encounter identifiers, a unified event timestamp, and event-type-specific code fields along with the required numerical attributes, enabling consistent event-level representation across domains for downstream sequence modeling.

### D.4.2 Downstream Cohorts

**Recurrent Acute Otitis Media (rAOM)** rAOM, or recurrent ear infection, is a common medical condition in early childhood. While most children will experience an ear infection during their first years of life, approximately 20-30% of the pediatric population will experience recurrent ear infections defined as 3 episodes within a 6 month period or 4 episodes within a year period. Children who experience rAOM often require surgical intervention in the form of ear tube placement. We sought to develop a predictive model for the probability a first AOM develops into rAOM.

We identified a cohort of 3,852 children with a first AOM. Of these, 22.0% transitioned into rAOM. We used the same embeddings framework as above to process prenatal, birth and developmental

clinical data. Since our eligible cohort had reached age 4 — an age at which rAOM is unlikely to developed — we modeled the binary diagnosis indicator as the outcome. Our training and testing sizes were 2,822 and 1,030, respectively.

**Autism Spectrum Disorder (ASD)** ASD is a neuro-developmental condition that typically presents within the first years of life. The mean age of the diagnosis is around 5 years. Children are typically screened during their 18-month well-child visit and referred for confirmatory diagnosis. Previous works has shown that early medical conditions (e.g., gastrointestinal disease) can serve as early indicators of a future ASD diagnosis. Our team has been focusing on developing automated early screening tools for ASD.

We identified a cohort of 43,945 children who had a well-child visit at our institution between 12 and 24 months of age. We used the well-child visits closest to 18 months as the index encounter. We required two distinct medical encounters with an ICD-10 for ASD to label an ASD case. Across our cohort’s follow-up, 2.05% were diagnosed with ASD. Our training and testing sizes were 35,000 and 8,945, respectively.

**30-day Hospital Readmission** Hospital readmission is a commonly used measure of short-term healthcare utilization and quality of care in pediatric populations. We focus on 30-day hospital readmission following emergency inpatient or inpatient hospitalization encounters among children.

We identified a cohort of 26,617 children who had at least one emergency inpatient (EI) or inpatient hospitalization (IP) encounter at our institution between January 1, 2016 and age 18. After excluding birth-related encounters, we used all qualifying EI or IP encounters with a discharge disposition of Home/Self Care (HO) or Home Health (HH) as index encounters, allowing multiple index encounters per patient. We defined the outcome as 30-day readmission, requiring the occurrence of a subsequent Emergency Department (ED), EI, or IP encounter within 30 days following discharge from the index encounter. The final cohort consisted of 45,755 index encounters, of which 19.1% were followed by a 30-day readmission. Our training and testing sizes were 33,683 and 12,072, respectively.

## D.5 Finetuning Model

Since we have optimized [CLS] embeddings, we adopt [CLS]-pool strategy on the set level. Following Rasmy et al. [28] and Odgaard et al. [23], we use a two-layer Bi-GRU as the downstream task model for both nonlinear probing and .

## E SoftCLT

Because event streams consist of categorical data, we cannot directly compute the pairwise distance matrices required for soft instance-wise contrastive loss. To address this, we attempted to extract continuous representations using the first half of the NEST block deck, where no dropout is applied, to derive soft labels via a distance matrix. Dropout is only applied in the second half of the deck for data augmentation [6]. However, the online calculation of Dynamic Time Warping (DTW) distance between latent states is computationally prohibitive, thereby negating the efficiency gains of the architecture. Consequently, we adopted the hard instance loss variant of SoftCLT. This approach eliminates the need for distance matrices and soft labels, relying instead on hard positive pairs formed between dropout-augmented representations.

We adopt the unsupervised SimCSE recipe (BERT with a linear-tanh projection head) [6] to pretrain the SoftCLT-based variant of our model, denoted as NEST<sub>SoftCLT</sub>. Following this approach, we optimize a contrastive loss alongside the MLM objective.

$$\mathcal{L} = \lambda \cdot \mathcal{L}_{\text{MLM}} + \mathcal{L}_{\text{SoftCLT}} \quad (\text{E.1})$$

Following the hyperparameter suggestions from SoftCLT [17] and SimCSE [6], we use the following configuration to calculate the loss terms. The MLM loss coefficient  $\lambda = 0.1$ , and hyperparameters in SoftCLT are configured as temporal contrastive temperature  $\tau_{\text{temp}} = 1$ , contribution coefficients for contrastive losses are 0.5 and 0.5. We do not need to specify  $\alpha$  as we use hard contrastive loss at instance level.